Steep X-ray reflection emissivity profiles in AGN as the result of radially structured disc ionization

Kammoun, E.S.; Domček, V.; Svoboda, J.; Dovčiak, M.; Matt, G.

DOI
10.1093/mnras/stz408

Publication date
2019

Document Version
Final published version

Published in
Monthly Notices of the Royal Astronomical Society

Monthly Notices
of the
ROYAL ASTRONOMICAL SOCIETY

MNRAS **485,** 239–247 (2019)
Advance Access publication 2019 February 14

doi:10.1093/mnras/stz408

Steep X-ray reflection emissivity profiles in AGN as the result of radially structured disc ionization

E. S. Kammoun [1,2★†], V. Domček [3,4], J. Svoboda,[5] M. Dovčiak[5] and G. Matt[6]

[1]*Department of Astronomy, University of Michigan, 1085 South University Avenue, Ann Arbor, MI 48109-1107, USA*
[2]*SISSA, via Bonomea 265, I-34135 Trieste, Italy*
[3]*Anton Pannekoek Institute / GRAPPA, University of Amsterdam, Science Park 904, NL-1098 XH Amsterdam, the Netherlands*
[4]*Department of Theoretical Physics and Astrophysics, Masaryk University, Kotlářská 2, CZ-611 37 Brno, Czech Republic*
[5]*Astronomical Institute of the Academy of Sciences, Boční II 1401, CZ-14100 Prague, Czech Republic*
[6]*Dipartimento di Matematica e Fisica, Università degli Studi Roma Tre, via della Vasca Navale 84, I-00146 Roma, Italy*

Accepted 2019 February 7. Received 2019 February 7; in original form 2018 July 23

ABSTRACT

X-ray observations suggest high compactness of coronæ in active galactic nuclei as well as in X-ray binaries. The compactness of the source implies a strong radial dependence in the illumination of the accretion disc. This will, for any reasonable radial profile of the density, lead to a radial profile of the disc ionization. Svoboda et al. showed on a single example that assuming a radially structured ionization profile of the disc can cause an artificial increase of the radial emissivity parameter. We further investigate how the X-ray spectra are modified and quantify this effect for a wide range of parameters. Computations are carried out with the current state-of-the-art models for relativistic reflection. We simulated spectra using the response files of the microcalorimeter X-IFU, which is planned to be on board of Athena. We assumed typical parameters for X-ray bright Seyfert-1 galaxies and considered two scenarios for the disc ionization: (1) a radial profile for the disc ionization and (2) a constant disc ionization. We found that steep emissivity profiles can be indeed achieved due to the radial profile of the disc ionization, which becomes more important for the cases where the corona is located at low heights above the black hole and this effect may even be more prominent than the geometrical effects. We also found that the cases with high inner disc ionization, rapidly decreasing with radius, may result in an inaccurate black hole spin measurements.

Key words: accretion, accretion discs – black hole physics – relativistic processes – galaxies: nuclei – X-rays: galaxies.

1 INTRODUCTION

X-ray spectroscopy of active galactic nuclei (AGNs) and X-ray binaries (XRBs) provides a good opportunity to study the physics of accretion on supermassive black holes (e.g. Brandt & Alexander 2015; Merloni 2016, and references therein). The X-ray emission originates in a hot medium (the so-called 'corona') located above the accretion disc consisting of relativistic electrons that inverse-comptonize the thermal ultraviolet light emitted by the accretion disc. The X-ray emission from the corona is partly emitted in the direction of the observer (known as 'primary spectrum') and partly in the direction of the accretion disc, as shown in Fig. 1. In the latter case, the light will be reprocessed by the accretion disc and re-emitted towards the observer (known as 'reflection spectrum'). The evidence for such reflected emission from the accretion disc is the presence of broad fluorescent iron Kα lines (at $\sim$6.4 keV), in addition to a broad hard X-ray excess peaking at 20–30 keV (known as Compton hump) reported in X-ray spectra of several AGN (e.g. Tanaka et al. 1995; Walton et al. 2012; Marinucci et al. 2014b; Parker et al. 2014; Svoboda et al. 2015)

Measuring the properties of X-ray radiation from the innermost regions allows us to constrain the properties of the corona and gives a potential way to estimate black hole spins (for a review see e.g. Reynolds 2013 and references therein). AGN X-ray spectra showing broad iron lines need, therefore, to be fitted with models that account for the relativistic effects, such as the gravitational and Doppler frequency shifts, light bending, aberration, and Doppler boosting. Several numerical codes have been developed in order to estimate these relativistic effects on the X-ray reflection spectra and can be used for spectral fitting (e.g. Beckwith & Done 2004; Dovčiak, Karas & Yaqoob 2004b; Brenneman & Reynolds 2006; Niedźwiecki & Życki 2008; Dauser et al. 2010; Niedźwiecki,

★ E-mail: ekammoun@umich.edu
† Former PhD student at SISSA.

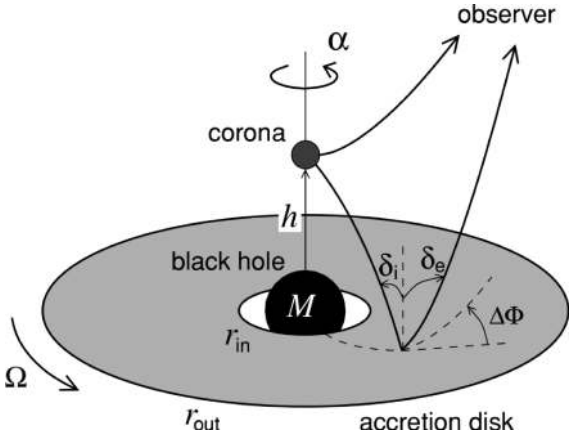

Figure 1. Lamp-post geometry scheme (figure adapted from Dovčiak et al. 2011).

Zdziarski & Szanecki 2016). The ultimate goal of such analyses is to measure the black hole spin. However, such measurements are strongly affected by a mutual degeneration of the model parameters. The spin measurements depend on the inclination of the system (Beckwith & Done 2004; Dovčiak et al. 2004b), and also on parameters that account for the geometry of the corona, namely the X-ray reflection emissivity profiles (see e.g. Beckwith & Done 2004; Svoboda et al. 2009, 2012), reflection fractions (Dauser et al. 2014), or directly the height of the corona (Dovčiak et al. 2014; Kammoun, Nardini & Risaliti 2018), assuming the so-called lamp-post geometry as shown in Fig. 1.

The lamp-post geometry is a simplification of a compact centrally located corona that has been suggested mainly from the measurements of a steep radial emissivity of X-ray spectra of several AGNs and XRBs. The emissivity index q describes how much the reflected emission decreases with the radius (see equation 1). Steep indices were commonly measured in Seyfert 1 galaxies. For example, Walton et al. (2013) showed that 15/25 bare AGNs, from their sample, reveal steep emissivities, larger than 5 (see their tables 2 and 3). Five other cases in their samples had emissivities indices steeper than 4, while they could not constrain the emissivity profiles for rest of the sources so they fixed it to 3. More recent measures have also shown steep emissivities in AGNs, for example, 1H0707-495 ($q_{\rm in} = 10.2^{+0.8}_{-0.9}$, $q > 8.6$, $q = 7.3^{+0.4}_{-0.2}$; Dauser et al. 2012; Fabian et al. 2012a; Kosec et al. 2018, respectively), IRAS 13224-3809 ($q_{\rm in} = 7.6^{+0.5}_{-0.2}$; Jiang et al. 2018), Mrk 335 ($q_{\rm in} \sim 7.7$–9.9; Wilkins & Gallo 2015), or Swift J2127.4 + 5654 ($q = 6.3^{+1.1}_{-1.0}$; Marinucci et al. 2014a). The steep emissivity in X-ray reflection spectra was also found in several cases of black hole XRBs, such as Cyg X-1 ($q_{\rm in} > 7$; Fabian et al. 2012b; Tomsick et al. 2014), GRS 1915 + 105 ($q_{\rm in} > 7$; Miller et al. 2013), MAXI J1535-571 ($q_{\rm in} = 7.8$; Miller et al. 2018), XTE J1650-500 ($q \approx 4$–5; Miniutti, Fabian & Miller 2004), or GX 339-4 ($q \approx 6$; Miller 2007).

The measured indices often reach values up to $q \approx 7$–10, which can be hardly explained without requiring an extremely compact X-ray source (Svoboda et al. 2012; Dauser et al. 2013; Dovčiak et al. 2014), or an extended corona but at a very low height above the inner disc (Wilkins & Fabian 2011; see Section 2.1 for further discussion regarding the various emissivity laws and geometries.). Another independent indication of the compactness of the corona comes from the gravitational microlensing of quasars. Recent results from monitoring observations of lensed quasars showed that the X-ray corona can indeed be confined within a half-light radius of $\sim 6\,r_g$ (Chartas et al. 2009; Mosquera et al. 2013; Reis & Miller 2013). The compact X-ray source has to cause a significant radial profile of the disc irradiation. Consequently, when any realistic profile of the density is considered, the ionization also significantly decreases with the radius (Svoboda et al. 2012). This effect is, however, totally neglected in the current spectral fittings, which assume a constant ionization of the accretion disc that is fitted as an independent parameter. This may then break the self-consistency of the models, thus leading to inaccurate physical interpretations. Svoboda et al. (2012) showed on a simple example that ignoring this effect may indeed cause measurements of artificially steeper radial emissivity indices for a case of highly compact corona located at low height, assuming a lamp-post geometry. In this work, we significantly extend the previous analysis by performing a systematic analysis of this effect. For this reason we consider different configurations of lamp-post height, disc ionization, and disc density. We further investigate in more details how these factors may affect the measurements of emissivity profiles as well as the spin parameter.

2 MODEL ASSUMPTIONS

2.1 Lamp-post scheme of the corona and radial emissivity profile

The lamp-post scheme of the corona (George et al. 1989; Matt, Perola & Piro 1991), as shown by a schematic illustration in Fig. 1, represents the simplest geometry of a compact X-ray source. The idea of a compact X-ray source positioned on the rotational axis of the black hole was also used to explain the observed X-ray variability of AGN (Miniutti & Fabian 2004; Niedźwiecki & Miyakawa 2010). The flux decreases when the height of the corona decreases because of the larger photon capture by the central black hole. Moreover, at low heights, more primary radiation will be focused towards the innermost regions of the accretion disc due to light-bending and gravitational redshift that decreases the reflected flux as well (see e.g. Martocchia & Matt 1996). The reflection fraction therefore increases in this state (for quantitative estimates see e.g. Dauser et al. 2013).

However, in a more realistic situation the corona may be a more complex inhomogeneous medium extended in both radial and vertical direction to larger radii (e.g. Wilkins & Gallo 2015). Dovčiak & Done (2016) pointed out that the source needs to be extended to be able to produce sufficiently enough X-ray photons to match the observations. However, the more complex models that would account for the spatial extension of the corona would contain more free parameters that would be difficult to be uniquely constrained with the current quality of the data. Therefore, owing to its simplicity, the lamp-post scheme is still popular and frequently used in the most recent codes for relativistic smearing (Dauser et al. 2013; Dovčiak et al. 2014). Besides to an isotropic homogeneous corona, the lamp-post scheme represents a simple approximation of a spatially compact corona, which is concentrated towards the centre.

Often, instead of assuming any particular geometry, the radial emissivity profile, with an emissivity index q, was introduced in the relativistic reflection models:

$$\epsilon(r) \propto r^{-q}. \quad (1)$$

For an isotropic corona, the thermal energy dissipation is assumed to decrease with the third power of radius ($q = 3$), following the standard prescription of the accretion disc temperature (Shakura &

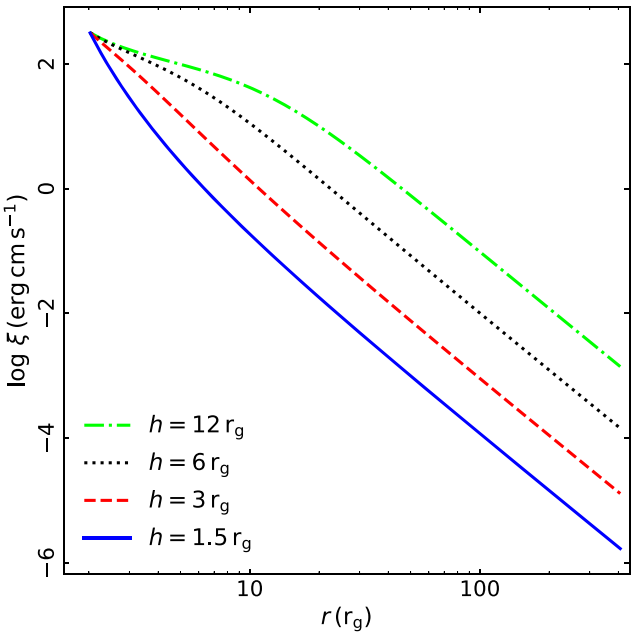

Figure 2. The radial ionization profile $\xi(r)$, estimated using the KYNXILLVER model, for various lamp-post heights 1.5 r_g (solid blue line), 3 r_g (dashed red line), 6 r_g (dotted black line), and 12 r_g (dash-dotted green line). We assume the same inner ionization parameter ($\log \xi_{in} = 2.5$) for all the cases.

Sunyaev 1973). Also, for the lamp-post geometry, the irradiation at distant parts of the accretion disc should follow r^{-3} (Reynolds & Begelman 1997). Thus, $q = 3$ is considered as a 'standard' index of the emissivity. However, the emissivity profile in the lamp-post geometry significantly changes in the innermost regions depending on the location of the X-ray source (see e.g. Martocchia, Karas & Matt 2000; Martocchia, Matt & Karas 2002; Wilkins & Fabian 2011; Dauser et al. 2013; Dovčiak et al. 2014). Assuming an accretion disc with a constant density and ionization, q can reach large values only when the source is located very close to the black hole event horizon. In this case, the emissivity profile is very steep at the innermost radii, then it flattens and finally reaches $q = 3$ at further radii, where the contribution to the total reflection spectrum is often relatively small. Therefore, with the current quality of the data, broken (or twice-broken) power laws can be used as adequate approximations of the intrinsic emissivity profiles (e.g. Wilkins & Fabian 2012; Gonzalez, Wilkins & Gallo 2017).

2.2 Disc irradiation and the ionization profile

The accretion disc material, irradiated by the X-ray photons of the corona, will then be naturally ionized, depending on the illuminating flux. The strong radial dependence of the irradiation, discussed in the previous section, will consequently lead to a radial dependence in terms of ionization as well. Therefore, the ionization parameter (ξ) at each radius, r, of the disc can be described as

$$\xi(r) = \frac{4\pi F_{\rm inc}(r)}{n_{\rm H}}, \qquad (2)$$

where $F_{\rm inc}$ is the irradiating flux and $n_{\rm H}$ is the density of the disc, assumed to be a constant. Fig. 2 shows the dependence of the ionization profile on the height of the lamp-post. By increasing the height of the lamp-post further out regions of the disc are illuminated, which leads to a flattening in the ionization profile below ∼20 r_g. In the radial extension, this assumption is satisfied because the radial dependence of the irradiation is much stronger than the radial dependence of any realistic density profile (see fig. 3 in Svoboda et al. 2012).

The vertical structure of the disc would cause that the reflection at each radius is composed of reflection from different layers and thus with different ionizations (e.g. Zycki et al. 1994; Nayakshin, Kazanas & Kallman 2000; Ballantyne, Ross & Fabian 2001). However, we simply assume that more ionized emission would still more likely come from the innermost regions where the irradiation is much higher due to light bending. Thus, the decrease of the reflection emission with radius, for an average ionization level, should be preserved similar to the case without any vertical structure. Considering the vertical stratification of the disc density would then require employing more complex models that are not currently available for the fast spectral fitting required in this analysis. Therefore, we potentially left studying the effect of vertical stratification for future investigations.

In this work, we used the XILLVERD (García et al. 2016) tables for the ionized reflection model. This model assumes a power-law primary illuminating an accretion disc for a given ionization parameter and density. We note that the effect of ionization is the most prominent below ∼10 keV. For the cold/neutral disc (low ξ_d), a number of emission lines are expected in the soft X-rays. As the disc gets warmer and more ionized, the equivalent width of the emission lines decreases. In the most ionized case, no lines originate by reflection from such ionized plasma. We note that different ionization levels also influence the shape of the reflection spectrum. While the highly ionized reflection spectra resemble a power-law shape decreasing with the energy, the cold reflection spectra have less emission in the soft band and a more prominent Compton hump. Consequently, there is a lower spectral power-law index when comparing the cold and highly ionized reflection. We also note that the larger the disc density the larger the soft flux (below ∼1 keV). This is attributed to an increase in the surface temperature of the disc as the density increases (see García et al. 2013; García et al. 2016, for more details about the effect of disc ionization and density on the reflection spectrum).

2.3 Relativistic reflection combining the lamp-post geometry and radially structured ionized reflection

By combining the relativistic smearing code from the KYN package (Dovčiak et al. 2004a) and the ionized reflection model, we get the resulting model KYNXILLVER,[1] which incorporates both the lamp-post geometry (Dovčiak et al. 2014) and the radially structured ionization, self-consistently calculated from the X-ray irradiation. It also includes the primary power-law continuum that goes directly to the observer. The model can be described as

$$\texttt{KYNXILLVER} = \texttt{powerlaw} + \sum \texttt{KYNCONV}(\Delta r_i) * \texttt{XILLVER}(\xi_i). \qquad (3)$$

It represents the total X-ray emission of the source and reflection from the accretion disc with different ionization level in each annulus. The primary flux is assumed to be isotropic in the local frame of the lamp-post. In other words, the amount of radiation emitted, per solid angle, in the direction of the observer is same as the one emitted in the direction of the disc. This can be done by setting the KYNXILLVER parameter $\texttt{N}p : Nr = 1$. The model then accounts self-consistently for the relativistic effects acting on the primary radiation, depending on the height of the source.

[1] https://projects.asu.cas.cz/stronggravity/kyn#kynxillver

Table 1. Key parameters used to perform the simulations with the corresponding input range.

Parameter	Input value
a^*	0.94
M ($M_\odot$)	10^7
θ (deg.)	30
$r_{\rm in}$ ($r_{\rm ISCO}$)	1
$r_{\rm out}$ (r_g)	400
$\log\left(\frac{\xi_{\rm in}}{\rm erg\ cm\ s^{-1}}\right)$	0–4.5
h (r_g)	[1.5, 3, 6, 12]
Γ	2
$A_{\rm Fe}$ (solar)	1
$n_{\rm H}$ ($\rm cm^{-3}$)	10^{15-19}

3 METHODS

3.1 Data simulation

The spectral simulations and the consequent analysis were performed using a combination of the software tools for X-ray spectral analysis `XSPEC V12.10` (Arnaud 1996) and Python as the XSPEC's wrapper and plotting device. First we created theoretical spectra assuming the following seed model (in the XSPEC terminology),

$$\texttt{model}_{\rm seed} = \texttt{phabs} \times \texttt{KYNxillver}, \quad (4)$$

where the phabs model accounts for the photoelectric absorption that is present in the line of sight of our Galaxy (we assume a column density $N_{\rm H} = 4 \times 10^{20}\,\rm cm^{-2}$). Throughout our analysis, we used values of typical X-ray bright Seyfert 1 galaxies presented in Table 1. We note that the parameters of the KYNXILLVER model that are not presented in this table are fixed to their default values. We considered five values for the disc density in the range $10^{15} - 10^{19}\,\rm cm^{-3}$, four lamp-post heights $h = 1.5, 3, 6, 12\,r_g$. We modified the intrinsic luminosities of the primary source as defined by the KYN model in a way that, for each case, the inner value of the ionization parameter at the innermost stable circular orbit (ISCO) $\log\xi_{\rm in}$ is between 0 and 4.5 (we considered 10 values of $\log\xi_{\rm in}$ spaced by a step of 0.5). Fig. 3 shows the total observed 2–10 keV flux for each of the considered cases. Our aim is to investigate how the radial emissivity parameter changes in response to different heights of the corona and different densities of the accretion disc by simulating spectra of bright local AGN. For that reason we chose only the cases that represent a flux level between 10^{-12} and $10^{-10}\rm erg\,s^{-1}\,cm^{-2}$, plotted as blue points in Fig. 3. We note that this figure clearly shows the restrictions in the parameter space that are present in flux-limited samples. For example, for low density ($n_{\rm H} = 10^{15}\,\rm cm^{-3}$) and low height ($h = 1.5\,r_g$), the intrinsic luminosity has to be small in order to have accretion discs with mild ionization ($\log\xi_{\rm in} = 2$, for example). This would result in low observed flux $\sim 10^{-15}\rm erg\,s^{-1}\,cm^{-2}$. Such sources, if they exist, cannot be detected with reasonable exposures. Studying various configurations and their observational implications are beyond the scope of this work and left for future investigations.

Then, we used the XSPEC command fakeit to create fake spectra based on the blue points in Fig. 3, considering the response files of the X-ray Integral Field Unit (Ravera et al. 2014) that will be on board of the planned ESA mission *Athena* (Nandra et al. 2013). We assumed exposure times of 100 ks, with no background files. The spectral analysis throughout this work is performed using the Cash statistics (C −stat; Cash 1976) without rebinning the spectra or the response files.

3.2 Spectral analysis model

The data were created using a complex model with variable radially structured ionization of the disc. However, for the spectral analysis we used a simpler model (in the XSPEC terminology):

$$\texttt{model}_{\rm fit} = \texttt{phabs}\times(\texttt{KYconv * atable\{xillverD-4.fits\}} + \texttt{powerlaw}), \quad (5)$$

where KYconv is a convolution model that we apply to the XILLVERD reflection tables assuming a single power-law radial emissivity and a constant ionization of the disc, and the power-law component represent the primary emission. Such model configuration has been standardly used in the X-ray data analysis when relativistic reflection is taken into account (e.g. Ponti et al. 2010; Marinucci et al. 2014a; Kosec et al. 2018), and we aim to investigate how the emissivity index is affected if the intrinsic data are more complex with radially structured ionization.

Broken or twice-broken power-law emissivity profiles have also been used for X-ray spectral fitting with the relativistic reflection models since they better correspond to the emissivity profile of the source in the lamp-post geometry (Wilkins & Fabian 2011; Wilkins et al. 2014). The emissivity is very steep at the innermost region, then flattens and finally it follows r^{-3} profile. However, these more complex emissivity profiles may lead to a degeneracy between the emissivity indices and the break radii. Thus, assuming a single power-law emissivity profile diminishes a possibility that the best-fit would result in a steep emissivity index but in a very tiny area of the innermost region, and it is appropriate enough to understand the effect of the radial disc-ionization profile on the measured emissivity indices.

Our model has five free parameters, namely the spin ($a*$), the emissivity index (q), the ionization of the disc ($\xi_{\rm fit}$), and the normalizations of the power law ($N_{\rm PL}$) and the reflection ($N_{\rm XILLVER}$) components. The other parameters of the model were fixed to their input values. The fits were statistically accepted in most of the cases, except for the cases were the fluxes are very high $F_{2-10} \sim 10^{-10}\,\rm erg\,s^{-1}\,cm^{-2}$, where some residuals could be seen below ∼0.8 keV. We show two examples of the simulated spectra together with the corresponding best-fitting models in Fig. 4. These spectra were simulated assuming $\log\xi_{\rm in} = 2.5$ and densities $n_{\rm H} = 10^{18}\,\rm cm^{-3}$ and $n_{\rm H} = 10^{19}\,\rm cm^{-3}$, which according to Fig. 3 correspond to different flux level. The residuals at soft X-rays for the bright case ($n_{\rm H} = 10^{19}\,\rm cm^{-3}$) can be seen clearly in the middle panel of Fig. 4, while the residuals for the low-flux case can be well acceptable (see bottom panel of the same figure). This clearly demonstrates that the radially structured ionization can be easily undetectable in most of the data analysis. We further study how the parameters of the reflection model could change to mimic the intrinsic reflection emission with radially structured ionization.

4 RESULTS

The results obtained by fitting the simulated data with the model presented in equation (5) are shown in Fig. 5. The x-axis represents the inner ionization parameter that was used in the simulations. The plots show (from top to bottom) the best-fitting values of the emissivity index, ionization parameter of the constant-ionization model, spin, and the goodness of the fit (C-stat/dof). Different

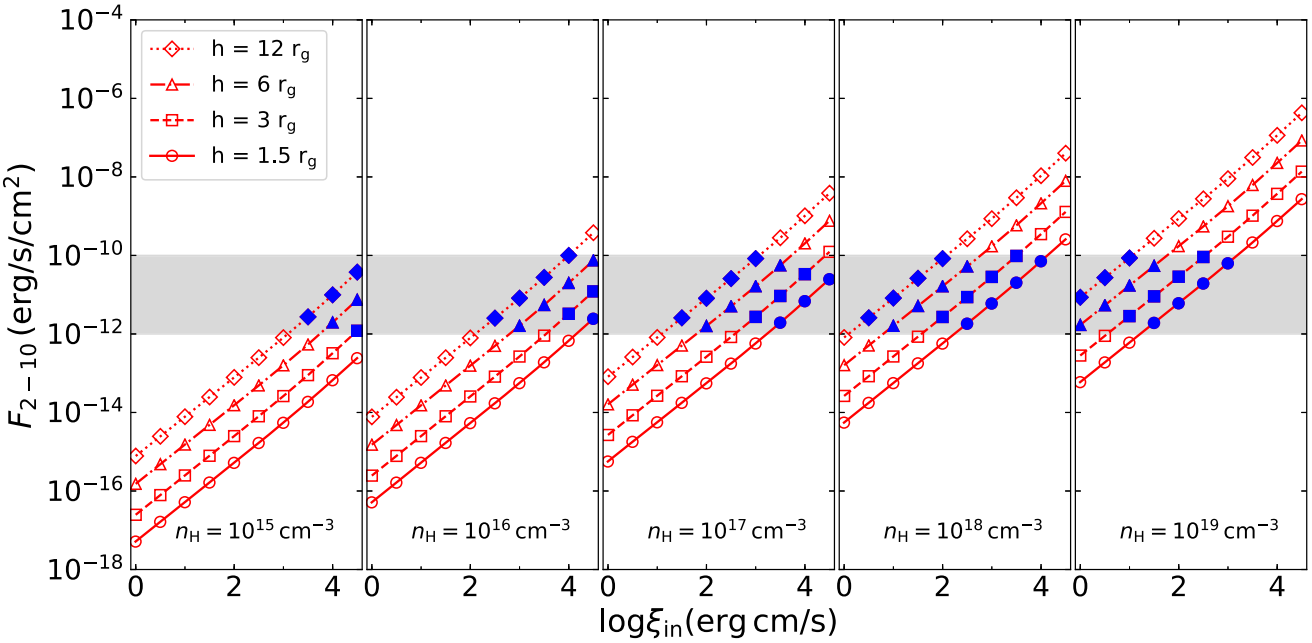

Figure 3. Observed 2–10 keV flux as function of the ionization parameter at the ISCO for the various values of $n_{\rm H}$ and h that are considered for this work. The shaded regions represent the flux range of $10^{-12} - 10^{-10}$ erg s^{-1} cm^{-2}. The blue points represent the cases that are simulated in this work (see Section 3.1 for more details.).

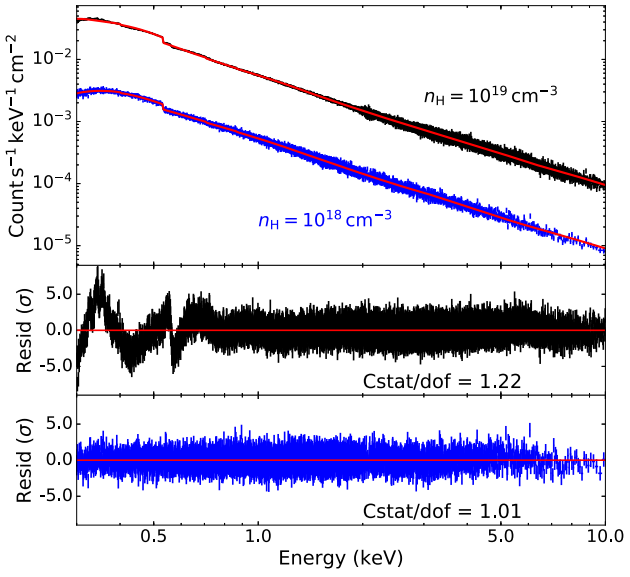

Figure 4. Simulated spectra assuming $\log \xi_{\rm in} = 2.5$, $h = 1.5\,{\rm r_g}$, and densities $n_{\rm H} = 10^{18}$ cm^{-3} (blue points) and $n_{\rm H} = 10^{19}$ cm^{-3} (black points) together with the correspondent best-fitting models (red lines). The residuals for the latter and former spectra are plotted in the bottom and middle panels, respectively. The spectra are binned for clarity.

heights were considered in the simulations ($h = 1.5$, 3, 6 and 12 r$_{\rm g}$ from left to right). The coloured (filled) symbols represent the cases for different accretion-disc densities and the radially structured ionization according to the lamp-post source illumination.

The emissivity index q increases up to ∼7 and ∼5 for heights of 1.5 and 3 r$_{\rm g}$, respectively, while it approaches the limit of q ∼ 3 for larger heights. In fact, q is low for $\log \xi_{\rm in} < 1.5$ and it increases with larger $\xi_{\rm in}$, then it again decreases for high values of $\log \xi_{\rm in} > 4$. This effect is an immediate consequence of the ionization gradient of the disc (shown in Fig. 2). For low and large values of $\xi_{\rm in}$, the parts of the disc contributing the most to the observed spectrum would be either neutral or highly ionized, depending on the height of the lamp-post. Thus, a very small gradient of ionization would be expected in these parts of the disc, and the constant-ionization approximation holds in these extreme cases, which apparently results in lower values of q. However, for the intermediate values of $\xi_{\rm in}$, the gradient of ionization is more important. The innermost regions will be more ionized and will have softer reflection spectra with respect to further out regions of the disc that are less ionized with a non-negligible contribution to the overall spectrum. Thus, a model assuming a single ionization parameter of the disc will underestimate the ionization from the innermost regions by assuming an average ionization. This effect will then be compensated by requiring a steep emissivity profile (see fig. 4 of Svoboda et al. 2012 for more details about how the reflection spectra look like for different radii with the radially decreasing ionization).

We note that the disc density plays a minor role in determining the emissivity profile. The values of q for different values of $n_{\rm H}$, assuming the same $\xi_{\rm in}$, are consistent with each other. This leave us with two interplaying factors that may affect the emissivity profile: (i) the geometry (height of the lamp-post) and (ii) the ionization gradient. In order to investigate which of the two factors, or if it is the combination of both, that is leading to steep emissivity indices we performed the following experiment. We followed the same procedure described in Section 3 but considering a constant ionization for the disc. In this case, both the simulations and the spectral fits are performed assuming a disc with a constant ionization. This will allow us to evaluate quantitatively how much the geometry of the source would play a role in giving rise to steep emissivity profiles. The best-fitting parameters are shown as open symbols in Fig. 5. The emissivity indices are almost constant for the various ionization states, assuming the same lamp-post height. The

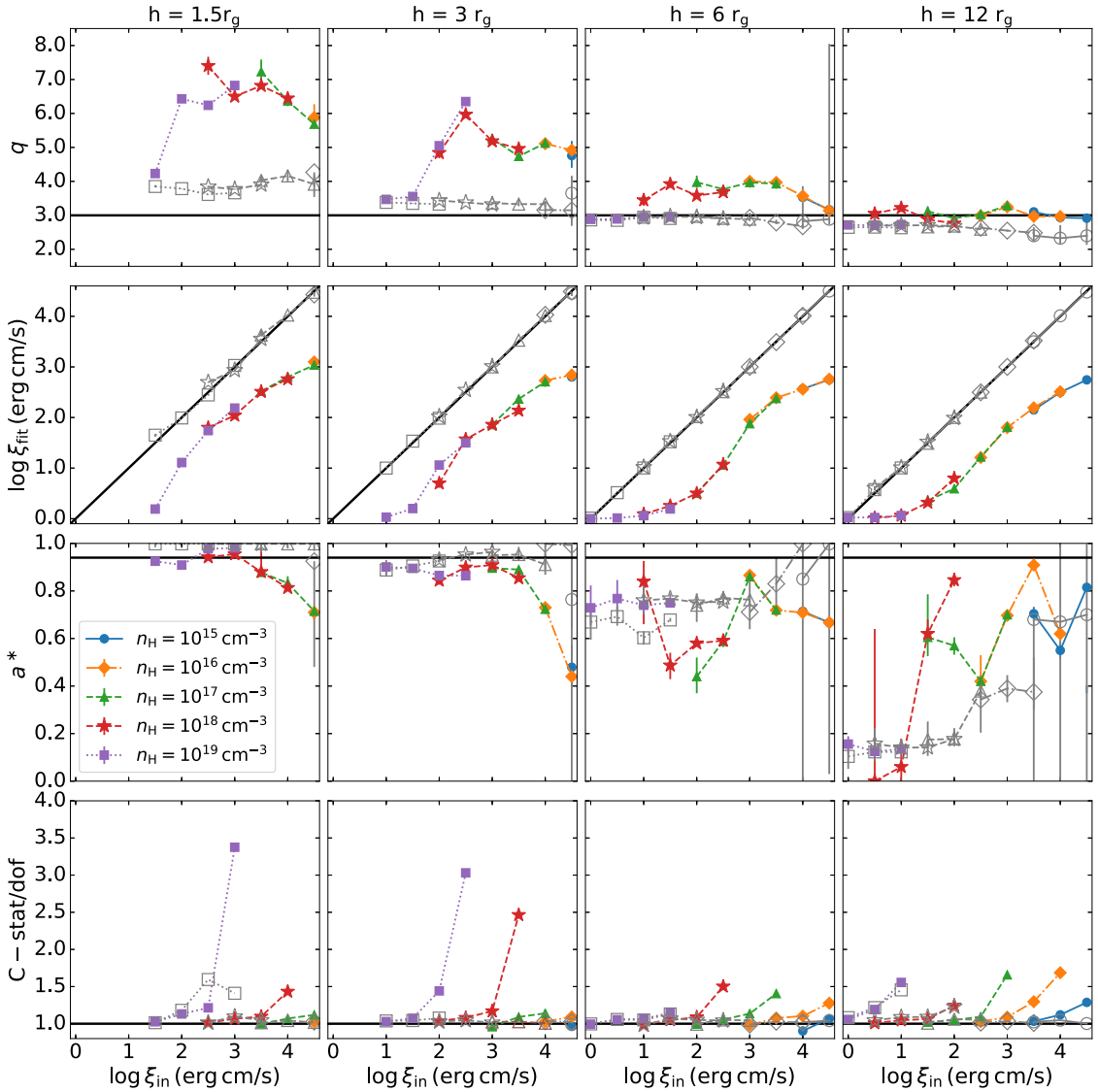

Figure 5. Best-fitting parameters, emissivity index, ionization parameter, spin parameter, goodness of fit (from top to bottom rows, respectively) obtained by fitting the simulated spectra for the various lamp-post heights and disc densities that we consider in this work. The simulations were performed assuming a radial ionization profile (filled symbols) and constant ionization (empty symbols) for the accretion disc. The black solid lines represent the identity line (upper row), the Newtonian limit for the emissivity profile ($q = 3$), the input value of the spin parameter ($a* = 0.94$), and C − stat/dof = 1 (top to bottom rows, respectively; See Section 4 for more details).

average values of q are 3.89, 3.35, 2.89, and 2.59 for $h = 1.5$, 3, 6, and 12 r_g, respectively. This clearly indicates that the steepening in emissivity profiles that can be introduced *only* by the geometry of the corona is much smaller than the one introduced by considering the radial profile of the disc ionization as well.

The third key parameter in our analysis is the black hole spin. It is clear from the lower panel of Fig. 5 that the correct value of $a* = 0.94$ can be recovered for the cases of low heights (1.5 and 3 r_g). While for larger heights, the spectral fits suggest lower and unconstrained spin values. This effect has been already discussed by several previous works and attributed to the fact that for larger heights, further out regions of the disc would be illuminated thus contributing more to the observed spectra, which makes it less probable to recover the correct value of the spin (Dovčiak et al. 2014; Fabian et al. 2014; Kammoun et al. 2018). We note that this effect is seen for both simulations (assuming a radial and constant ionization profiles). However, when fitted by a model with the constant ionization profile, the spin parameters are better constrained and consistent with the input values for low heights compared to the former case. This indicates that the ionization profile of the disc has some non-negligible effect on the spin measurements.

More interestingly, we note that for the two low heights (1.5 and 3 r_g) the ability of recovering the correct spin value depends on the ionization of the disc (see Fig. 5). The measured spin values are lower for high-ionization states. This can be mainly due to the fact that for high ionizations the reflection features are smoothed out giving a power-law-like spectrum (see fig. 3 in García et al. 2013, for example). Therefore, we suggest that this may be caused by a degeneracy between the reflection and the power-law spectral components which may appear at such high ionization. As a result, the fitting procedure preferentially underestimates the reflection component. When the overionized reflection from the innermost

region is not any more modelled as reflection, the fit will then consider that the 'observed' reflection is emitted from further out regions of the accretion disc, thus requiring larger values of the ISCO (as compared to the true one). This consequently leads to smaller values of the spin estimates. We note that this applies only for the cases where the spectra were simulated assuming a radially structured disc ionization. While the cases assuming a constant ionization result in accurate spin measurements (see Fig. 5). This emphasizes the importance of considering radial profiles of ionization with respect to constant values, if this is the intrinsic profile. Otherwise, the spin measurements can be affected by the above-mentioned spectral model degeneracy.

5 DISCUSSION

In this work, we have studied the effect of a possible radial structure of the disc ionization on the other parameters of the relativistic reflection models, namely the emissivity index and the spin. The motivation for our work originates from the observationally suggested compactness of the disc-illuminating X-ray source. The innermost regions of the disc are illuminated by much stronger radiation than the outer parts of the disc, which naturally leads to the radial decrease of the disc ionization for any reasonable density profile of the disc, as illustrated by Svoboda et al. (2012; see also Fig. 2 in this work). The authors also showed that this radial structure in ionization may significantly affect the measured radial-emissivity parameter of the reflection model. However, this was shown only for a single and rather extreme example.

Here, we significantly extend the work presented in Svoboda et al. (2012) by performing a systematic analysis to explore a large range of the parameter space possessing values that allow for a significant detection of the relativistic reflection features with a reasonable exposure time and we study a possible effect of the disc density. We investigated different ionization profiles through assumptions of the disc densities ranging between 10^{15} and 10^{19} cm^{-3}, assuming inner ionization parameters ($\log \xi_{\rm in}$ at the ISCO) in the range 0–4.5. For each ionization profile of the disc, we performed simulations of the corona being at different heights, ranging between 1.5 and 12 r_g above the black hole, assuming a total observed flux range between 10^{-12} and 10^{-10} erg s^{-1} cm^{-2}, in the 2–10 keV band. First, we simulated spectra assuming a radial profile of the disc ionization and fitted the spectra with models assuming the constant ionization. Then, in order to investigate the role of the geometry in giving the steep emissivity profiles, compared to the radial ionization profiles, we simulated spectra assuming constant disc ionizations and fitted them using models assuming the same criterion. We found that the theoretically expected ionization gradient in the accretion disc leads to significantly steeper emissivity indices than simply the geometrical effects due to the lamp-post geometry (cf. coloured and grey curves in Fig. 5).

We stress that we do not present in this work any observational evidence of the detection of an ionization gradient profile in AGN accretion disc. Instead, our argument is based on simple physical implications of the lamp-post geometry configuration. Fig. 6 presents a *qualitative* comparison of our results to observational measures. The open symbols in this figure represent the measured emissivity index versus the ionization parameter from table 2 in Walton et al. (2013). We plot only the cases where at least a lower limit could be estimated for the emissivity index. We note that, interestingly, none of the observed ionization parameters in this sample correspond to a highly ionized or completely neutral accretion discs. For the sake of comparison and simplicity, we have divided the observed data points

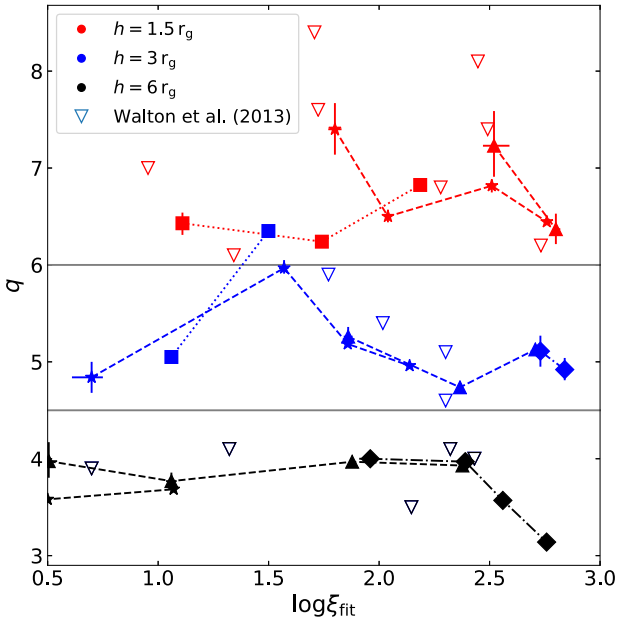

Figure 6. Best-fitting emissivity indices q as function of the best-fitting ionization parameter $\log \xi_{\rm fit}$ obtained from our simulations for lamp-post heights $h = 1.5,\ 3$ and $6\,r_g$ (black, blue, and red filled symbols, respectively). The various symbols correspond to different disc densities (using the same code as in Fig. 5). The open triangles correspond to the measured values obtained from Walton et al. (2013), where different colours correspond to different 'q-bands' (black: $q \leq 4.5$, blue: $4.5 < q \leq 6$, and red: $q > 6$; see the text for details).

into three emissivity-index bands: $q \leq 4.5$ (black open symbols), $4.5 < q \leq 6$ (blue open symbols), and $q > 6$ (red open symbols). The filled symbols in Fig. 6 correspond to our simulations presented in Fig. 5. We limit ourselves to the cases where we estimate $\log \xi_{\rm fit}$ to be in the 0.5–3 range, which broadly corresponds to the observed range for the sample in Walton et al. (2013). We show the cases that were simulated assuming $h = 1.5$, 3, and $6\,r_g$ (black, blue, and red filled symbols) for the various disc densities. This figure shows a fair (qualitative) agreement between the observed data and the results of our simulations that were initially modelled assuming a lamp-post with a self-consistently calculated ionization gradient of the disc. We note that many uncertainties may affect this comparison mainly whether the reflection strength/fraction would be consistent using the various configurations and models, in addition to the effects of the spin parameter. We note that further work will be needed to assess this issue, ideally requiring the (re-)analysis of the spectra within the context of a gradient ionization profile, which is beyond the scope of this work.

We note that while the consideration of the radial structure in the accretion-disc ionization is one step towards a more self-consistent description of X-ray reflection spectra, there are several other uncertainties that are mainly caused by our poor knowledge of the exact geometry of the system.

(i) An extended corona: we assumed here a lamp-post geometry of the corona for simplicity. However, a more realistic configuration is an extended corona (Wilkins & Fabian 2012; Dovčiak & Done 2016; Tamborra et al. 2018; Zhang 2018) that would result in a somewhat different illumination of the disc and thus to different ionization profile. However, models of irradiation by such an extended corona are not yet available for spectral fitting and are

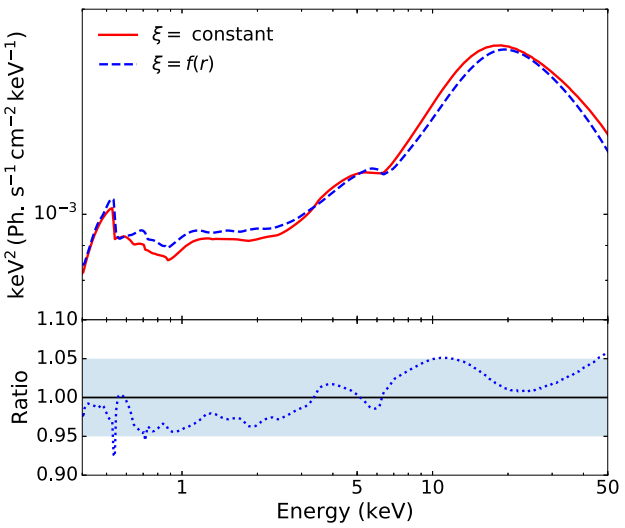

Figure 7. Input model used to simulate the data assuming an ionization gradient in the accretion disc with $h = 3\,r_g$, $\log \xi_{in} = 3$, and $n_H = 10^{17}$ cm^{-3} (dashed blue line) used to simulate the spectrum and the best-fitting model obtained by fitting the spectrum in the soft X-rays assuming a constant ionization (solid red line). We extrapolated both spectra to the hard X-rays in order to check whether the consistency remains at these energies. Bottom panel: The ratio between the two models (bottom panel) is within ∼5 per cent for the broad X-ray band.

dependent on the physical characteristics and structure of such coronæ.

(ii) An exact description of the accretion-disc density: we considered here a radial ionization gradient that is caused by the illumination of the disc with a constant density. Instead, a variation in the density profile of the disc is expected from theoretical models or GRMHD simulations (Novikov & Thorne 1973; Shakura & Sunyaev 1973; Penna, Sądowski & McKinney 2012). The exact ionization profile can be affected by the exact description of the disc density. However, the steep radial decrease of the illumination due to the growing distance from the source can hardly be compensated by a similarly steep increase of the density with radius. Our results are thus qualitatively independent of the accurate density description.

(iii) Variability: the primary emission is expected to be variable with time in flux and spectral shape. This would result in a variability in the ionization profile and in a further complexity in estimating the observed spectrum, especially when estimating the response of the accretion disc to any variation in the primary source. We do not consider these effects in this work.

(iv) Spin: we have limited our simulations to sources with a spin parameter of 0.94. Lower/higher spin values would result in larger/smaller values of the ISCO that will lead to different ionization profiles. These configurations are not considered in this work but should qualitatively provide similar results.

It is worth mentioning that our analysis is restricted to the soft X-ray band (below 10 keV). We performed a preliminary test, in order to check whether our results could be affected by including data at higher energies. We consider the case for $h = 3\,r_g$, $\log \xi_{in} = 3$, and $n_H = 10^{17}$ cm^{-3} in which the spectrum could be fitted by assuming a constant ionization parameter. In Fig. 7 we show the input spectrum that was used to simulate the data and the best-fitting model and we extrapolated both to the hard X-rays. The figure shows that a small difference (less than 5 per cent) is expected between the two models even at hard X-rays. We have tested the same for other configurations and they showed similar qualitative and quantitative behaviour. However, a more detailed analysis on how the various parameters might affect the hard X-ray spectra is left for future investigations.

Finally, we stress that our work is not discussing current ways of spin measurements using the constant ionization in the reflection model. In this work, we show, using high-sensitivity data with future planned instruments, that it is not easy to distinguish between a model with the ionization gradient and a model with the constant ionization and the steep radial emissivity for any set of parameters. Most fits with the constant ionization resulted in C-statistics *C/dof* $\lesssim$ 1.5 (see bottom panel of Fig. 5), thus providing with rather acceptable fits. However, we consider our work to be useful for understanding how the fitted parameters can be affected by our simplified model assumptions since the disc ionization gradient is a naturally expected consequence of the lamp-post geometry. Nevertheless, we plan to extend our work by applying our suggested model to the archival observational data from current instruments such as *XMM–Newton* and compare the results with those obtained here with simulated data for future X-ray mission *Athena*.

6 SUMMARY

X-ray reflection spectra in AGNs and XRBs are thought to originate thanks to the illumination of the accretion disc by a corona of hot electrons in the vicinity of the black hole. For a compact X-ray source located on the black hole rotational axis, this illumination will naturally decrease with radius, implying a radially structured ionization of the disc. We showed that such a decrease in ionization will result in measurements of steep radial emissivities ($q > 5$) assuming a model where the disc ionization is constant and fitted as an independent parameter. Steep emissivities are indeed measured in several sources, which may indicate the relevance of the combined effect of the lamp-post geometry and the ionization gradient. We note that many of these sources show a mild ionization state when fitted with a constant-ionization model, which along with the steep emissivity profiles could indicate the presence of a radial ionization gradient in the disc. Furthermore, we showed that the ionization gradient may affect the spin measurements as well. For highly ionized discs, the reflection features are smoothed out, which may result in inaccurate spin measurements if one assumes a constant ionization (this may underestimate the real contribution by reflection to the total spectrum). We also confirmed previous results stating that spin measurements would not be accurate if the corona is located at large heights. Finally, we showed that the level of the disc density does not play any important role in determining the emissivity profile.

ACKNOWLEDGEMENTS

We would like to thank the referee, Dr. Javier García, for useful comments and suggestions that helped improving the clarity of our manuscript. This work has been started during a visit, under the ERASMUS + Programme – Student Mobility for Traineeship-Project KTEU-ET (Key to Europe Erasmus Traineeship), of ESK to the Astronomical Institute of the Czech Academy of Sciences, whose hospitality he gratefully acknowledges. JS and MD acknowledge the financial support from the Grant Agency of the Czech Republic within the project No. 17-02430S and MEYS project LTAUSA17095.

REFERENCES

Arnaud K. A., 1996, in Jacoby G. H., Barnes J., eds, Astronomical Data Analysis Software and Systems V. Astron. Soc. Pac., San Francisco, p. 17

Ballantyne D. R., Ross R. R., Fabian A. C., 2001, MNRAS, 327, 10

Beckwith K., Done C., 2004, MNRAS, 352, 353

Brandt W. N., Alexander D. M., 2015, A&AR, 23, 1

Brenneman L. W., Reynolds C. S., 2006, ApJ, 652, 1028

Cash W., 1976, A&A, 52, 307

Chartas G., Kochanek C. S., Dai X., Poindexter S., Garmire G., 2009, ApJ, 693, 174

Dauser T., Wilms J., Reynolds C. S., Brenneman L. W., 2010, MNRAS, 409, 1534

Dauser T. et al., 2012, MNRAS, 422, 1914

Dauser T., Garcia J., Wilms J., Böck M., Brenneman L. W., Falanga M., Fukumura K., Reynolds C. S., 2013, MNRAS, 430, 1694

Dauser T., Garcia J., Parker M. L., Fabian A. C., Wilms J., 2014, MNRAS, 444, L100

Dovčiak M., Done C., 2016, Astron. Nachr., 337, 441

Dovčiak M., Karas V., Martocchia A., Matt G., Yaqoob T., 2004a, Processes in the Vicinity of Black Holes and Neutron Stars. Silesian University, Opava, p. 33

Dovčiak M., Karas V., Yaqoob T., 2004b, ApJS, 153, 205

Dovčiak M., Muleri F., Goosmann R. W., Karas V., Matt G., 2011, ApJ, 731, 75

Dovčiak M., Svoboda J., Goosmann R. W., Karas V., Matt G., Sochora V., 2014, in Stuchlík Z., Török G., Pecháček T., eds, Proc. RAGtime, An XSPEC Model to Explore Spectral Features from Black-Hole Sources - II. The Relativistic Iron Line in the Lamp-Post Geometry. Silesian University, Opava, p. 51

Fabian A. C. et al., 2012a, MNRAS, 419, 116

Fabian A. C. et al., 2012b, MNRAS, 424, 217

Fabian A. C., Parker M. L., Wilkins D. R., Miller J. M., Kara E., Reynolds C. S., Dauser T., 2014, MNRAS, 439, 2307

García J., Dauser T., Reynolds C. S., Kallman T. R., McClintock J. E., Wilms J., Eikmann W., 2013, ApJ, 768, 146

García J. A., Fabian A. C., Kallman T. R., Dauser T., Parker M. L., McClintock J. E., Steiner J. F., Wilms J., 2016, MNRAS, 462, 751

George I. M., Fabian A. C., Nandra K., Pounds K. A., Stewart G. C., 1989, in Hunt J., Battrick B., eds, ESA Special Publication Vol. 296, Two Topics in X-Ray Astronomy, Volume 1: X Ray Binaries. Volume 2: AGN and the X Ray Background. ESA, Paris

Gonzalez A. G., Wilkins D. R., Gallo L. C., 2017, MNRAS, 472, 1932

Jiang J. et al., 2018, MNRAS, 477, 3711

Kammoun E. S., Nardini E., Risaliti G., 2018, A&A, 614, A44

Kosec P., Buisson D. J. K., Parker M. L., Pinto C., Fabian A. C., Walton D. J., 2018, MNRAS, 481, 947

Marinucci A. et al., 2014a, MNRAS, 440, 2347

Marinucci A. et al., 2014b, ApJ, 787, 83

Martocchia A., Matt G., 1996, MNRAS, 282, L53

Martocchia A., Karas V., Matt G., 2000, MNRAS, 312, 817

Martocchia A., Matt G., Karas V., 2002, A&A, 383, L23

Matt G., Perola G. C., Piro L., 1991, A&A, 247, 25

Merloni A., 2016, Lecture Notes Phys., 905, 101

Miller J. M., 2007, ARA&A, 45, 441

Miller J. M. et al., 2013, ApJ, 775, L45

Miller J. M. et al., 2018, ApJ, 860, L28

Miniutti G., Fabian A. C., 2004, MNRAS, 349, 1435

Miniutti G., Fabian A. C., Miller J. M., 2004, MNRAS, 351, 466

Mosquera A. M., Kochanek C. S., Chen B., Dai X., Blackburne J. A., Chartas G., 2013, ApJ, 769, 53

Nandra K. et al., 2013, preprint (arXiv:1306.2307)

Nayakshin S., Kazanas D., Kallman T. R., 2000, ApJ, 537, 833

Niedźwiecki A., Miyakawa T., 2010, A&A, 509, A22

Niedźwiecki A., Życki P. T., 2008, MNRAS, 386, 759

Niedźwiecki A., Zdziarski A. A., Szanecki M., 2016, ApJ, 821, L1

Novikov I., Thorne K., 1973, in DeWitt C., DeWitt B., eds, Black Holes (Les Astres Occlus). Gordon and Breach, New York, p. 343

Parker M. L. et al., 2014, MNRAS, 443, 1723

Penna R. F., Sądowski A., McKinney J. C., 2012, MNRAS, 420, 684

Ponti G. et al., 2010, MNRAS, 406, 2591

Ravera L. et al., 2014, in Takahashi T., den Herder J.-W. A., Bautz M., eds, Proc. SPIE Conf. Ser. Vol. 9144, Space Telescopes and Instrumentation 2014: Ultraviolet to Gamma Ray. SPIE, Bellingham, p. 91442L

Reis R. C., Miller J. M., 2013, ApJ, 769, L7

Reynolds C., 2013, Space Sci. Rev., 183, 277

Reynolds C. S., Begelman M. C., 1997, ApJ, 488, 109

Shakura N., Sunyaev R., 1973, A&A, 24, 337

Svoboda J., Dovčiak M., Goosmann R., Karas V., 2009, A&A, 507, 1

Svoboda J., Dovčiak M., Goosmann R. W., Jethwa P., Karas V., Miniutti G., Guainazzi M., 2012, A&A, 545, A106

Svoboda J., Beuchert T., Guainazzi M., Longinotti A. L., Piconcelli E., Wilms J., 2015, A&A, 578, A96

Tamborra F., Matt G., Bianchi S., Dovčiak M., 2018, A&A, 619, A105

Tanaka Y. et al., 1995, Nature, 375, 659

Tomsick J. A. et al., 2014, ApJ, 780, 78

Walton D. J., Nardini E., Fabian A. C., Gallo L. C., Reis R. C., 2012, MNRAS, 428, 2901

Walton D. J., Nardini E., Fabian A. C., Gallo L. C., Reis R. C., 2013, MNRAS, 428, 2901

Wilkins D. R., Fabian A. C., 2011, MNRAS, 414, 1269

Wilkins D. R., Fabian A. C., 2012, MNRAS, 424, 1284

Wilkins D. R., Gallo L. C., 2015, MNRAS, 449, 129

Wilkins D. R., Kara E., Fabian A. C., Gallo L. C., 2014, MNRAS, 443, 2746

Zhang W., 2018, 42nd COSPAR Scientific Assembly. Pasadena, California, p. E1.4–52

Zycki P. T., Krolik J. H., Zdziarski A. A., Kallman T. R., 1994, ApJ, 437, 597

This paper has been typeset from a TEX/LATEX file prepared by the author.